Stanford Exploration Project, Report 92, November 12, 1997, pages 53–79

Stanford Exploration Project, Report 92, November 12, 1997, pages 53–79

Reservoir monitoring: A multi-disciplinary feasibility study

Biondo Biondi,[1] *David Lumley,*[2] *Gary Mavko,*[3] *Tapan Mukerji,*[4]
James Rickett[5]
Geophysics Department
—
Clayton Deutsch,[6] *Runar Gundesø,*[7] *and Marco Thiele*[8]
Petroleum Engineering Department

ABSTRACT

Monitoring reservoir changes with time-lapse seismic holds the promise to significantly improve reservoir characterization and reservoir management. To relate time-dependent changes in seismic to the underlying geological description and flow processes requires input from a number of disciplines: (1) geological modeling/geostatistics, (2) flow simulation, (3) rock physics, and (4) seismic imaging. This paper documents the start of a project that brings these disciplines together. In this initial model study we have considered the forward problem, i.e., create a detailed geological truth model, perform flow simulation, relate the dynamic rock properties to seismic properties, and, finally, image the reservoir at multiple times. We document this forward modeling exercise on a single geological relization and discuss opportunities for future work.

INTRODUCTION

There is a recognized need to combine the skills of geoscientists and engineers to build quantitative reservoir models that incorporate all available reservoir data. These integrated reservoir models are critical for forecasting, monitoring, and optimizing reservoir performance over the life cycle of the reservoir. They will enable reservoir engineers to more accurately perform flow simulation studies, identify permeability

[1]Stanford Exploration Project - email: biondo@sep.stanford.edu
[2]Chevron, Consulting Professor with the Geophysics Department. - email: luml@chevron.com
[3]Stanford Rock Physics and Borehole Project - email: gary@pangea.stanford.edu
[4]Stanford Rock Physics and Borehole Project - email: mukerji@pangea.stanford.edu
[5]Stanford Exploration Project - email: james@sep.stanford.edu
[6]Stanford Center for Reservoir Forecating - email: clayton@pangea.stanford.edu
[7]Norsk Hydro, visiting the Petroleum Engineering Department. - email: rgu@nho.hydro.com
[8]Stanford Univ. Petroleum Research Institute - Project B - email: marcot@pangea.stanford.edu

flow-paths and barriers, map bypassed oil, and monitor pressure and saturation fronts in the reservoir. All of these are essential for effective reservoir management.

Available reservoir data include conceptual geological models, seismic data, core data, well log data, and historical production data. Each data type carries information, at different scales and with varying levels of uniqueness, related to the true distribution of petrophysical and fluid properties in the reservoir. The *challenge* is to integrate all of these disparate data into a unified, self-consistent reservoir model. Such a challenge can only be tackled by collaborative efforts among specialists in the different disciplines.

This paper reports on the beginning of a joint reservoir modeling effort among four research groups in the Stanford School of Earth Sciences: SCRF-Stanford Center for Reservoir Forecasting, SUPRI-B- Stanford University Petroleum Research Institute (Reservoir Simulation), SRB-Stanford Rockphysics and Borehole Geophysics Project, and SEP-Stanford Exploration Project. For many years these groups have been studying different aspects of characterizing and modeling reservoirs, with varying amounts of collaboration. For example, SRB and SEP, along with Norsk Hydro, carried out a seismic monitoring feasibility study of the Troll field, involving reservoir modeling and flow simulation, rock physics, and seismic modeling (Lumley et al., 1994). SCRF and SUPRI-B have collaborated on building optimum stochastic reservoir models for flow simulation studies. SRB and SCRF are collaborating on how to more effectively and more properly use rock physics and seismic data to constrain geostatistical estimations and simulations. Our approach in the new work reported here was to involve all of the groups in a more systematic way, at all levels of the modeling project.

The work presented is aimed particularly at reservoir production monitoring, involving time lapse or 4-D seismic modeling. The value of repeated 3-D seismic surveys is that they allow us to subtract away much of the geologic uncertainty in the reservoir and overburden, while highlighting temporal changes in reservoir conditions related to production.

One of the goals was to lay the foundations for future collaborative projects among the participating groups and to foster a multi-disciplinary research and teaching environment. The definition of a common data flow and hardware platform is one essential requirement for an effective collaboration among research groups involved in analyzing and modeling large quantities of data. In this project we built tools for exchanging data and sharing software. This sharing was greatly facilitated by the availability of a single computational platform, a 16-processors Power Challenge from Silicon Graphics. This powerful machine was also necessary for the computationally intensive tasks of the project, such as the reservoir geological modeling, fluid flow simulation, and the seismic modeling and imaging.

This article demonstrates a methodology applied to a realistic model study. Our ultimate goal is to apply the method to data acquired on a real reservoir.

RESERVOIR MONITORING MODEL STUDY

Reservoir monitoring by repeated seismic surveys is based on the assumption that changes in fluid properties cause detectable changes in the recorded seismic data. For an individual reservoir under study the validity of this assumption depends on many factors, such as lithology, fluid properties, production history, and seismic data quality. To analyze the influence that all these factors have on the potential success of seismic monitoring, we developed numerical tools for modeling all the relevant physical processes involved in reservoir monitoring and linked them in a unified modeling flow.

The starting point of our project was building a reservoir model, shown in Figure **??**, whose lithology and structure resembles a North Sea reservoir. We then simulated the multiphase fluid flow and production history of the reservoir over a period of 3 years. We estimated the effective seismic properties of the reservoir combining the lithologic model and the fluid properties. Finally, we simulated multi-offset 3-D seismic surveys at different times during the production history. This process is shown as Steps A-D in Figure **??**.

While the macro-scale of our model reservoir is constant (5×5 km) the sampling of the reservoir physical parameters varies greatly between steps. The main scales that we used are described below:

Core Scale is about $0.1 \times 0.1 \times 0.1$ m. Much of what is known about rock physics relations among rock, fluid, and seismic properties has come from measurements at the core scale. Description of the complete reservoir at this scale would yield 10^{13} (10,000 billion) voxels and is not practical. Nevertheless, in any reservoir, a subset of core data can yield seismic-to-reservoir properties relations that are critical to the seismic modeling.

Reservoir Geological Modeling Scale is nominally $5.0 \times 5.0 \times 0.5$ m. Ideally, the geological model would be at the resolution of the best information, i.e., the core data. This is not practical and, instead, a scale is chosen small enough to capture the significant geological heterogeneities and large enough to yield a tractable number of cells or voxels. The scale chosen here yields 200 million voxels which is ambitious but practical for reservoir modeling. There are about 50,000 core scale voxels within a geological modeling cell.

Reservoir Flow Simulation Scale The scale of the grid blocks in fluid flow simulation is a compromise between the desire to minimize artificial numerical artifacts, accounting for sufficient geological detail, and available computational resources. Full-field simulation, requiring order 10^2 grid blocks between wells can easily lead to systems with 10^6–10^8 grid blocks, which remains well beyond current computational possibilities. In this study, a discretization of the macro-scale into nx=132 $\times$ ny=140 $\times$ nz=12 resulted in grid blocks with an areal scale

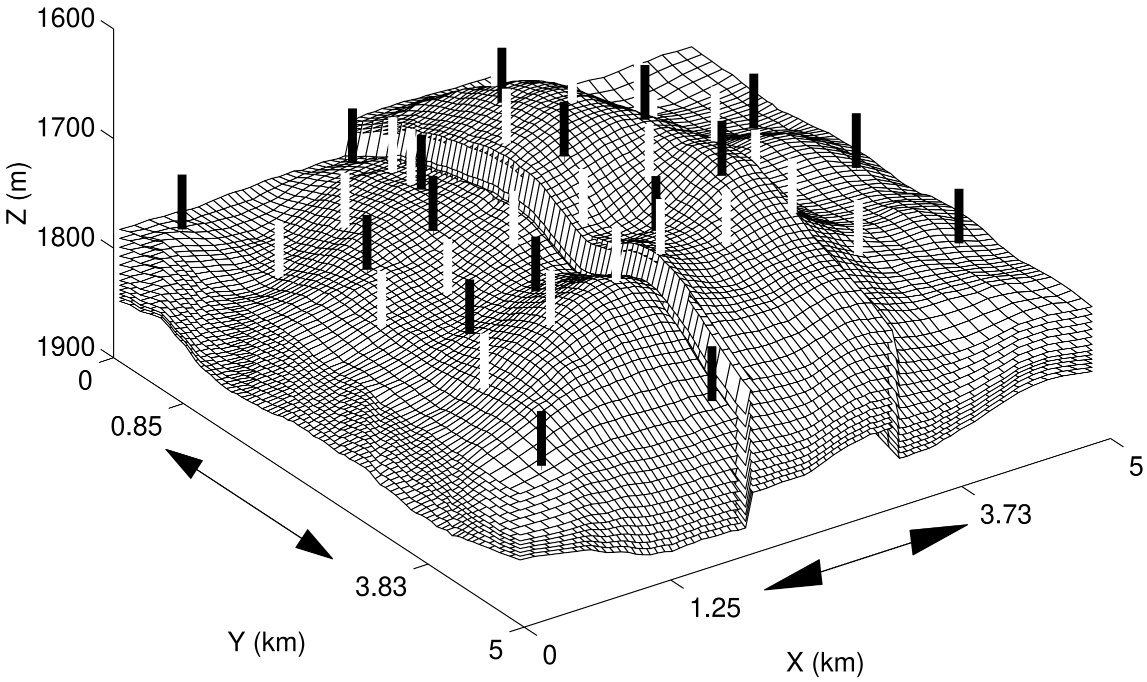

Figure 1: Perspective view of the reservoir model, showing structure and faults. The reservoir lithology was fashioned after braided stream fluvial reservoirs common in many parts of the world including the North Sea. Production wells are indicated in white, and water injection wells are indicated in black. Arrows and ticks along the X and Y axes show extent of seismic imaging. $\boxed{\text{biondo3-meshbw}}$ [NR]

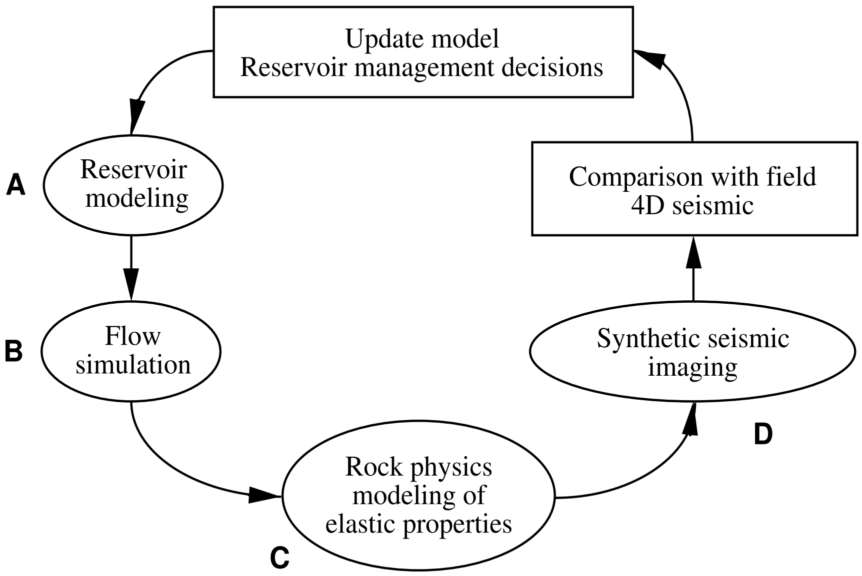

Figure 2: Steps involved in monitoring reservoir performance. biondo3-flow [NR]

of 62.5×62.5 m in the coarse region and 31.25×31.25 m in the refined region. The vertical size of the grid blocks, on average, was 8.3 m.

Seismic Imaging Scale is the scale of the resolution of the seismic images, that is linked with the wavelength of the seismic signal recorded at the surface (≈ 50 m in our model). We described the seismic properties of the reservoir on a $5 \times 5 \times 5$ meters scale. Description at this scale of the whole reservoir would yield about 50 million voxels. We have used a subset of the whole reservoir, for a total of about 1.5 million voxels.

RESERVOIR GEOLOGICAL MODELING

Size and resolution of geological model

A numerical geological model of a braided stream fluvial reservoir with an average net-to-gross ratio (proportion of channel sand) of 0.65 was constructed with no well or seismic conditioning data. The physical dimensions of the 200 million cell model are:

X	5 km	1000 x 5 m
Y	5 km	1000 x 5 m
Z	100 m	200 x 0.5 m

The vertical cell size is nominally 0.5 m; however, it varies areally to accommodate variation in the thickness from 80 m to 120 m.

High-resolution sequence stratigraphy, made possible by dense 3-D seismic and close-distance well logging data, reveals a reservoir framework composed of repetitive strata bounded by time-correlatable or chronostratigraphic surfaces. These strata often contain facies that contrast drastically in petrophysical properties such as permeability and porosity. It is necessary to treat these surfaces as first order heterogeneities for reservoir description and fluid flow modeling. In this modeling exercise, the 100 m vertical extent was modeled with three geological strata with 0.8, 0.4, and 0.6 net-to-gross ratios (proportion of channel sand) respectively. The top panel of Figure **??** shows a cross section through one layer.

Facies model

Once these strata or layers are identified, the distribution of channel complexes versus overbank deposits within each strata represents second order heterogeneities. The distribution of individual channels within each channel complex constitutes third order heterogeneities. Sequence stratigraphy allows such hierarchical classification of heterogeneities down to the bed set or bed level. This genetic hierarchy of heterogeneities within a given reservoir is best modeled through a hierarchical procedure. A hierarchical object-based procedure was applied to model the channel sand distribution in each layer. The key geologic input parameters are (1) the proportion of channel sand that could vary vertically and areally, (2) geometric parameters defining the channel thicknesses, widths, and sinuosities, and (3) well data. In this case, the layer proportions were assumed constant, realistic channel geometries were considered, and no well data were used to constrain the model. The second panel of Figure **??** shows a cross section through the channel and overbank shale facies model.

Porosity and permeability

A constant porosity of 15% and permeability of 0.01 md was assigned to the overbank shale deposits. Although the total porosity of the overbank shales was considered to be 15%, the effective porosity was considered to be 0%. Within the channel sands, porosity was assigned with sequential Gaussian simulation (SGS). The SGS algorithm constructs a stochastic porosity model constrained to a histogram of porosity, a model of spatial correlation, and well data. In this case, realistic input statistics were chosen on the basis of published North Sea reservoir examples. The histogram of porosity is shown on Figure **??**. The third panel of Figure **??** shows a cross section through the porosity model.

Finally, permeability was related to porosity through a scatterplot. Figures **??** and **??** give the histograms and porosity-permeability scatterplot.

Scale up

The flow simulation blocks for the 200,000 block model are approximately 1000 times larger than the geological model. The details in the geological model provide the ground truth petrophysical properties and are transferred to flow simulation as effective block properties. The scaled-up porosity was taken as the arithmetic average of the constituent porosity values (the fourth panel of Figure **??** shows a cross section through the scaled up porosity model), the scaled-up horizontal permeability was taken as the arithmetic average of the constituent permeability values, and the scaled-up vertical permeability K_v was taken as a power average of the n constituent permeability values K_i, $K_v = [\sum_i^n K_i^\omega]^{\frac{1}{\omega}}$, with $\omega = -0.2$. This power average for the vertical permeability takes into account that the flow paths are more tortuous in the vertical direction because of lateral continuity.

FLUID-FLOW SIMULATION

All fluid-flow simulations were done using the 1996A version of Eclipse, a three-phase, three-dimensional, general purpose black-oil simulator from GeoQuest. Black-oil is a term used to describe a set of simplifying assumptions used for modeling hydrocarbon phase behavior, in which all components are lumped into two pseudocomponents, oil and gas. Unfortunately, the words gas and oil are also used to distinguish between the vapor and liquid phase, sometimes confusing the uninitiated reader. Water is usually present as a third component and phase. The bulk of fluid flow simulations in the industry are done using the black-oil model.

GEOMETRY AND GRIDDING

Two models were simulated for this study. The first model consisted of nx=66, ny=70, and nz=12 grid blocks resulting in a total of 50,674 active cells. In the second model the number of blocks in the x and y directions were doubled to nx=132 and ny=140. The number of blocks in the vertical direction was kept at nz=12, leading to a total of 202,696 active cells. Active cells are cells with a porosity greater than 10^{-6}. Results of this second model were used in the seismic processing part of the study. Both models were gridded using a Cartesian geometry, with a denser grid at the center of the system (Figure **??**). The simulated area had an areal extent of 5 km $\times$ 5 km, and a thickness varying between 80 m and 120 m.

Two vertical faults were introduced in the yz-plane with an offset of 30 m. The faults were located at $x = 1,812.5$ m and $x = 3,375$ m. To account for the proper connections across the faults a total of 1,260 non-neighbor connections were introduced in the 50,674–cell model and 2,520 non-neighbor connections in the 202,696–cell model. Non-neighbor connections are required when blocks which are neighbors in the i, j, k ordering used as input are not neighbors in the actual physical space as, for example,

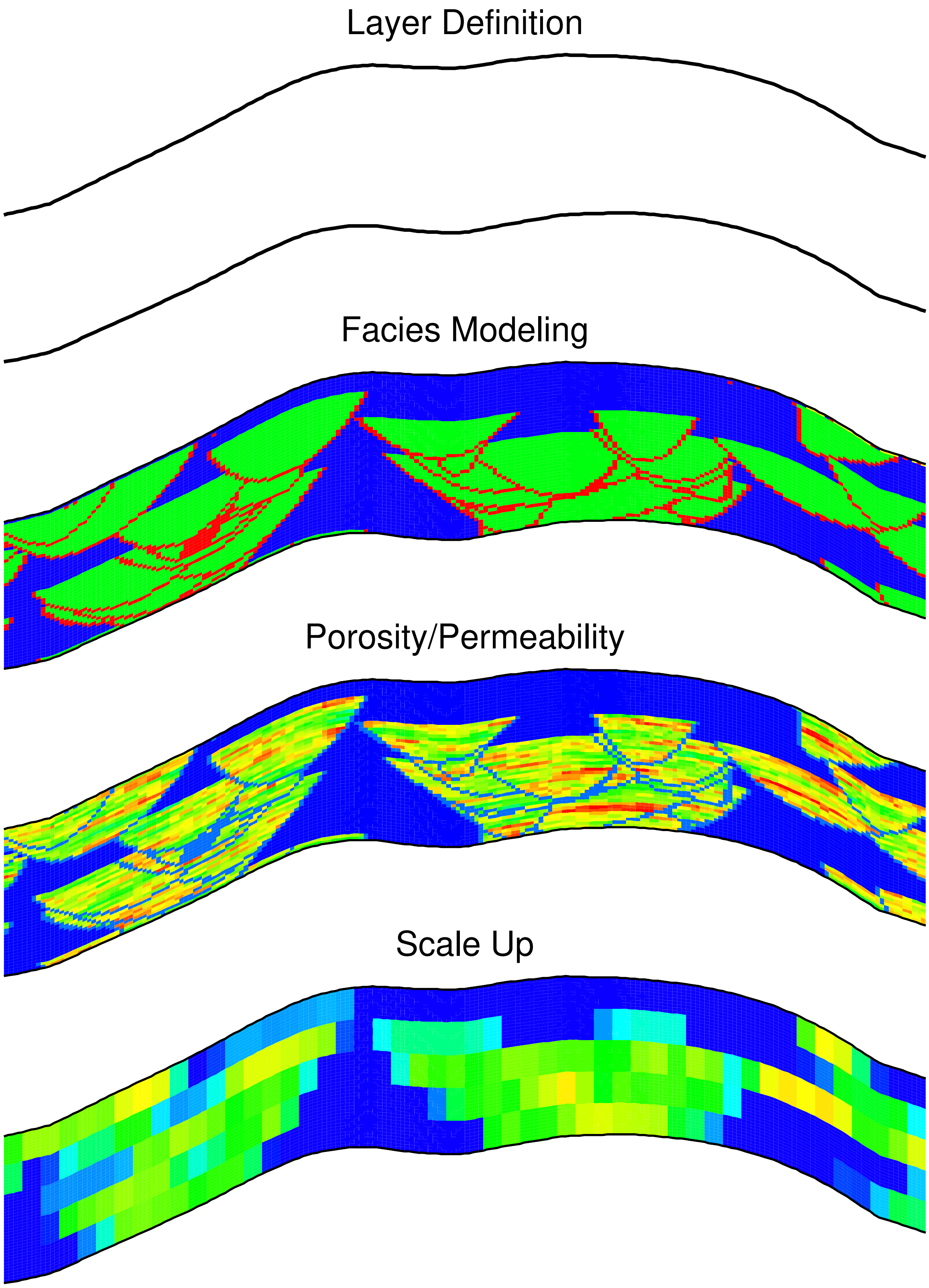

Figure 3: The steps in constructing the numerical geological model: (1) layer definition, (2) object-based channel modeling, (3) cell-based porosity and permeability modeling, and (4) scale up to a resolution for flow simulation. biondo3-secview [NR]

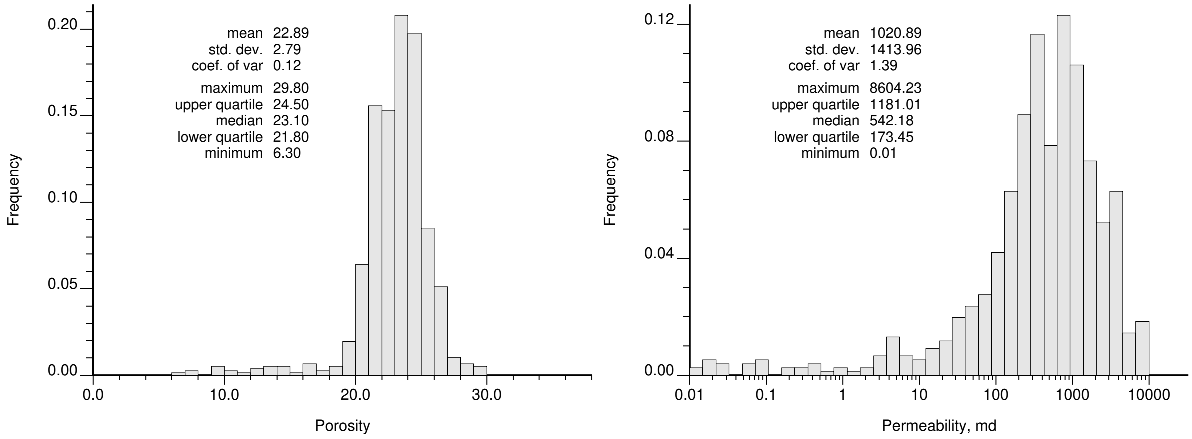

Figure 4: Histograms of porosity and permeability within channel sand. biondo3-histplt [NR]

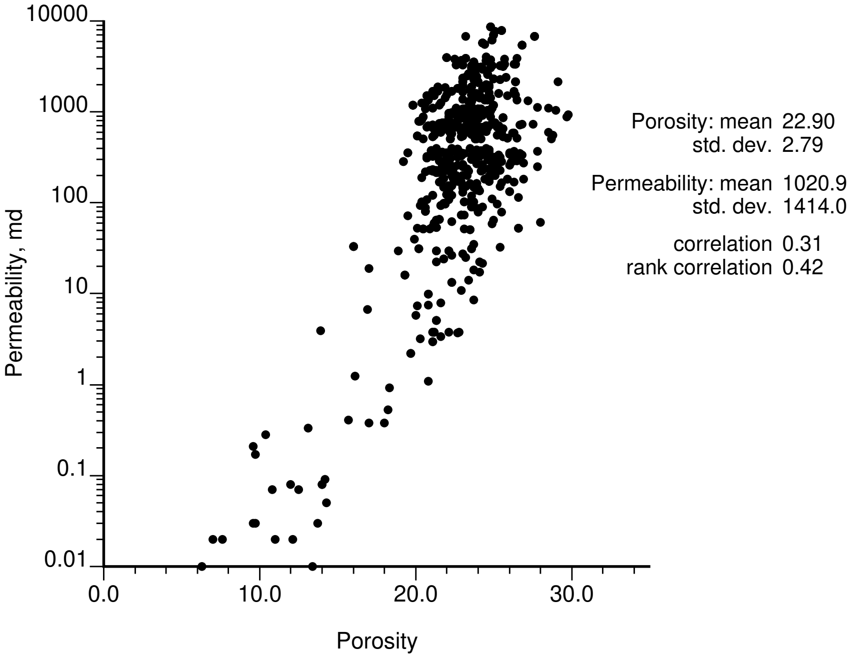

Figure 5: Scatterplot of porosity and permeability within channel sand. biondo3-scatplt [NR]

in the case of faults. Transmissibilities across the faults were then multiplied by 10 (at $x = 1,812.5$ m) and by 10^{-5} (at $x = 3,375$ m), thereby increasing the transmissibility of the first fault while almost sealing the second fault. Figure **??** shows the areal view of the top layer and a xz-slice at $y = 2,270$ m.

PVT-PROPERTIES

Properties for the simulations used in this study were picked to resemble a North Sea oil. The input of the phase behavior for black-oil models is in terms of formation volume factors, B_j, component solubilities, $R_{i,j}$, and phase densities at standard conditions, $\bar{\rho}_j$, (1 atm and 15°C). The insitu phase densities ρ_j, which are required for determining seismic properties, can always be recovered using

$$\rho_j = \frac{1}{B_j}\left(\bar{\rho}_j + \bar{\rho}_i R_{i,j}\right) \quad . \tag{1}$$

Formation volume factors for oil and gas as well as the solubility of the gas component into the oil phase, $R_{g,o}$, generally denominated as R_s, are shown in Figure **??**. The oil component was assumed to be present in the oil phase only ($R_{o,g} = 0.0$ for all pressures). The phase densities at standard conditions for oil, gas, and water were taken to be $\bar{\rho}_o = 876.2$ kg/m^3, $\bar{\rho}_g = 0.732$ kg/m^3, and $\bar{\rho}_w = 1024$ kg/m^3 respectively.

FLOW PROPERTIES

The effective permeability of the rock to a phase is taken as the product of the absolute permeability times the relative permeability of the phase which is a function of saturation. Relative permeabilities used in the simulations are shown in Figure **??**, and were taken from a North Sea data set. Relative permeabilities for water and gas are assumed to be a function of their own saturations only. The oil relative permeability is calculated from two sets of oil relative permeabilities using

$$k_{ro} = \omega_1 k_{rog} + \omega_2 k_{row} \quad , \tag{2}$$

where k_{rog} is the relative permeability of oil in the presence of gas and connate water, k_{row} is the relative permeability of oil in presence of water and no gas, and ω_1 and ω_2 are weighting functions given by

$$\omega_1 = \frac{S_g}{S_g + S_w - S_{wc}} \quad , \quad \omega_2 = \frac{S_w - S_{wc}}{S_g + S_w - S_{wc}} \quad . \tag{3}$$

S_g is the gas saturation, S_w is the water saturation, and S_{wc} is the connate water saturation. This is the default model used by Eclipse. Capillary pressure was assumed to be zero between all phases, and phase viscosities were set constant and equal to $\mu_w = 1.0$ cp, $\mu_o = 0.7$ cp, and $\mu_g = 0.02$ cp.

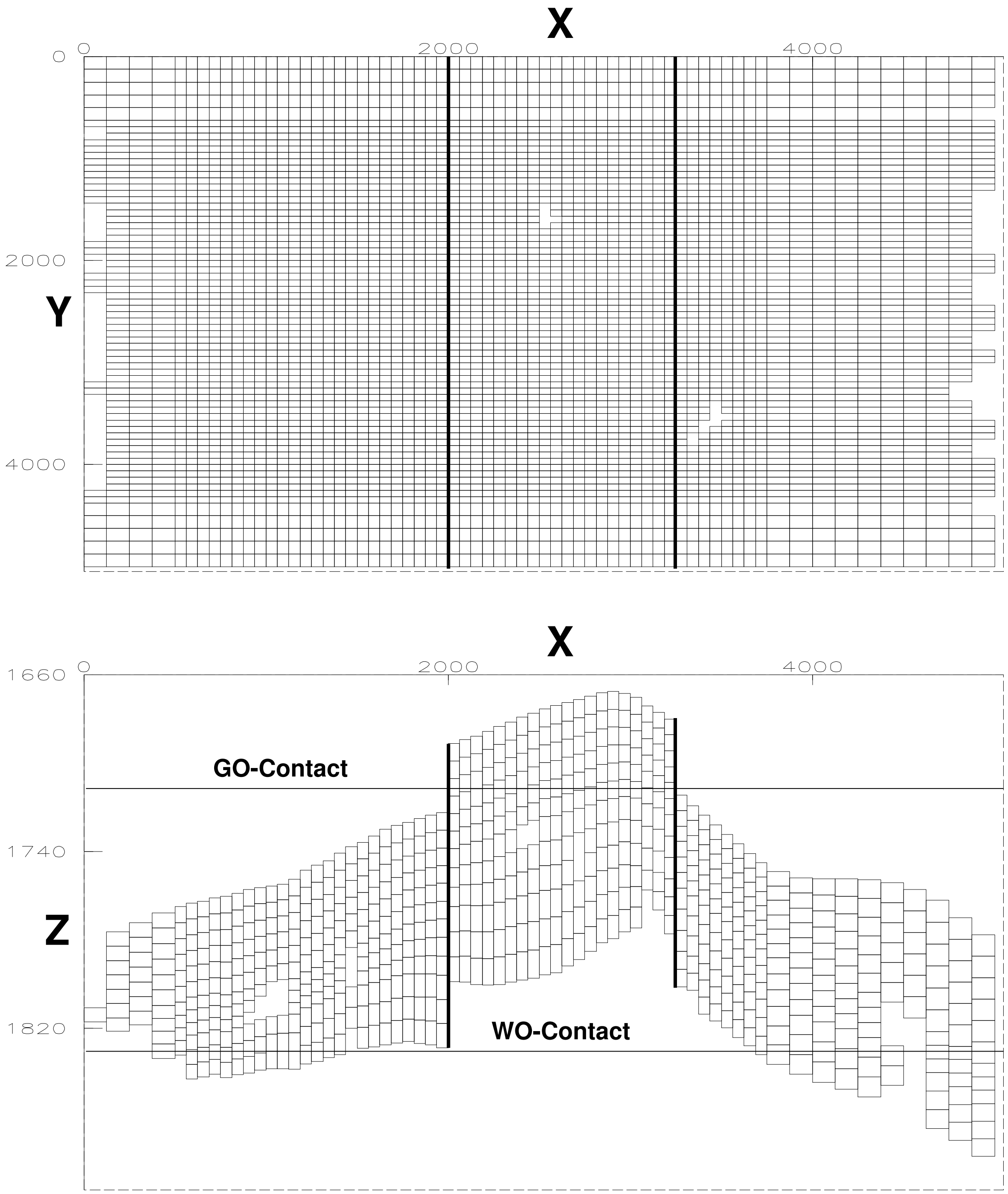

Figure 6: Areal and cross-sectional ($y = 2270$ m) meshing of the 50674–cell model, showing locations of faults and the gas–oil and water–oil contacts. The larger 202,696–cell model was constructed by doubling the number of grid blocks in the x– and y–directions. biondo3-marcofig2 [NR]

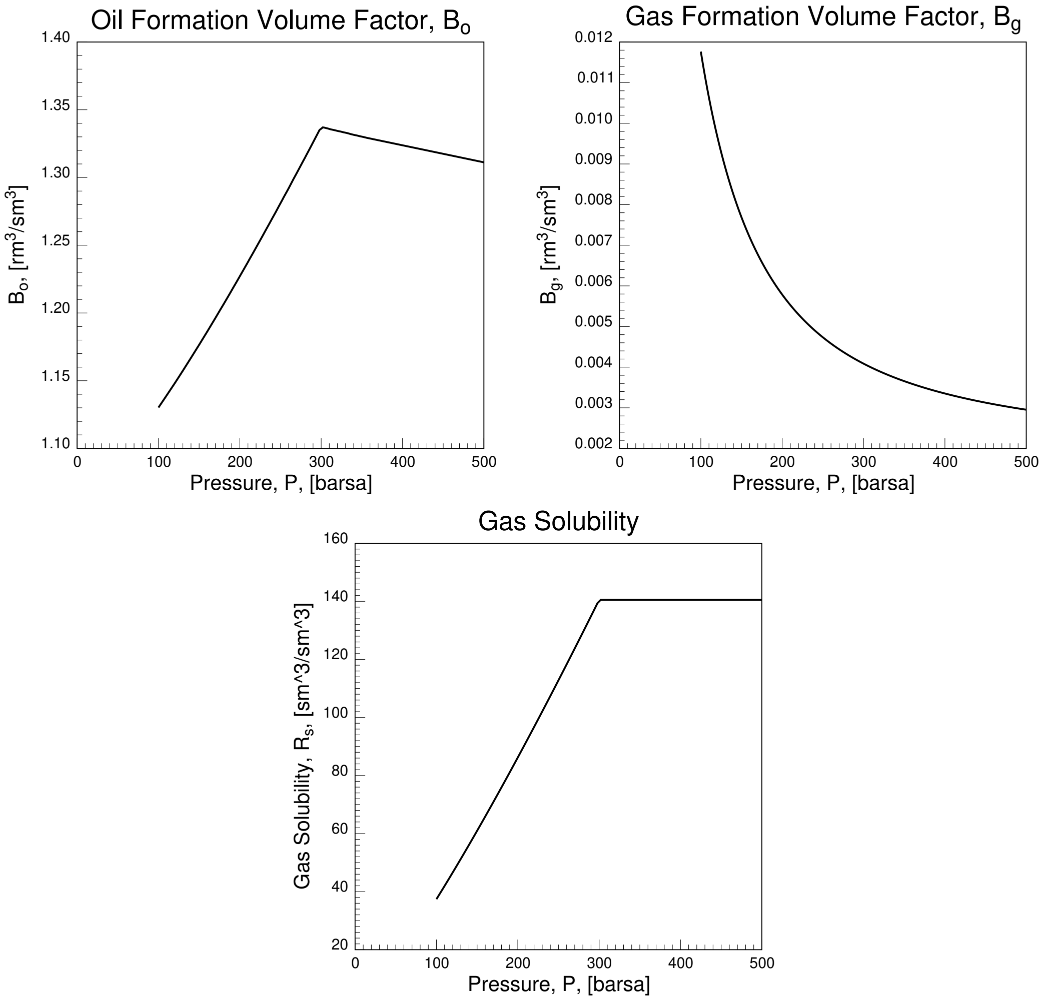

Figure 7: Oil and gas formation volume factors and gas solubility as a function of pressure. Solubility of oil into the gas phase was assumed zero. The water component is assumed present in the water phase only. $\boxed{\text{biondo3-marcofig1}}$ [NR]

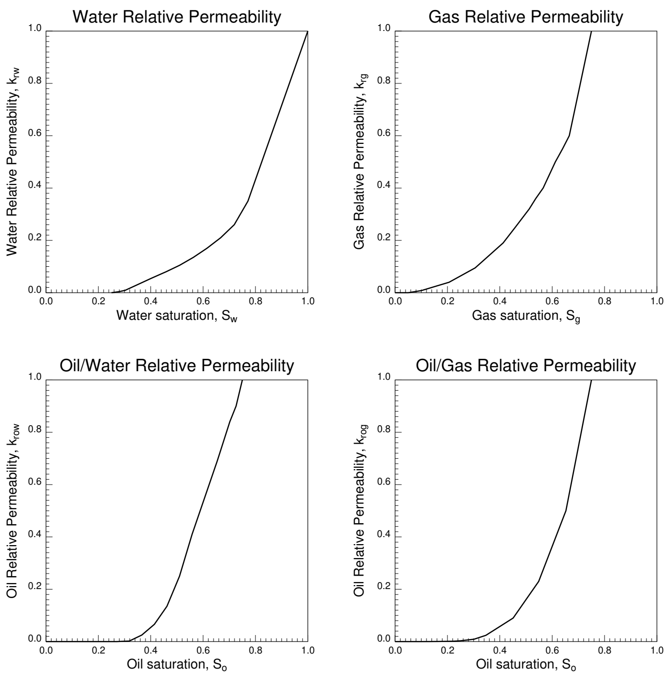

Figure 8: Relative phase permeabilities from a real North Sea data set used for the fluid-flow simulations. biondo3-marcofig3 [NR]

Models	$66 \times 70 \times 12$	$132 \times 140 \times 12$
Memory	122 MB	441 MB
Simulation time	3 Years	3 Years
V. Produced	0.248 PV	0.246 PV
CPU Time (1)	2.2 hr	71.0 hr
CPU Time (2)	1.1 hr	—
CPU Time (4)	0.71 hr	—
CPU Time (8)	0.40	—

Table 0.1: Memory use and CPU-times for the fluid flow simulations. Numbers in parenthesis indicate number of processors used.

SIMULATION

The system was initialized using a datum pressure of 300 bars at the gas-oil contact at a depth of 1710 m. The water-oil contact was at 1830 m.

The reservoir was produced under primary production for the first 6 months using 24 production wells producing at 5000 m^3/day and a minimum bottom-hole pressure constraint of 200 bars. After 6 months of primary production, 17 injection wells were added injecting water at 5000 m^3/day with a maximum bottom-hole pressure constraint of 400 bars. The total simulation time was 3 years. Only vertical wells were included in the simulation.

Example fluid distributions at 3 years for a vertical cross-section and a horizontal slice are shown in Figures **??** and **??**. Water injection has clearly reduced the size of the gas cap (Figure **??**), and water injection is seen to be influenced by gravity, as shown by the cone-like pattern around the injection wells (Figure **??** a).

MEMORY AND TIMING

The Table 0.1 summarizes performance data for the simulations, which were performed on an Silicon Graphics Power Challenger with 16 processors and 2 GB of RAM. All results used in this study were obtained using a single processor. Some preliminary performance results for the parallel version of Eclipse, based on PVM and a distributed memory algorithm, are also given. The number of CPUs used is given in parenthesis.

ROCK PHYSICS MODELING

Rock physics provides the link between reservoir properties and the seismic properties that can be observed with a geophysical survey. The reservoir parameters

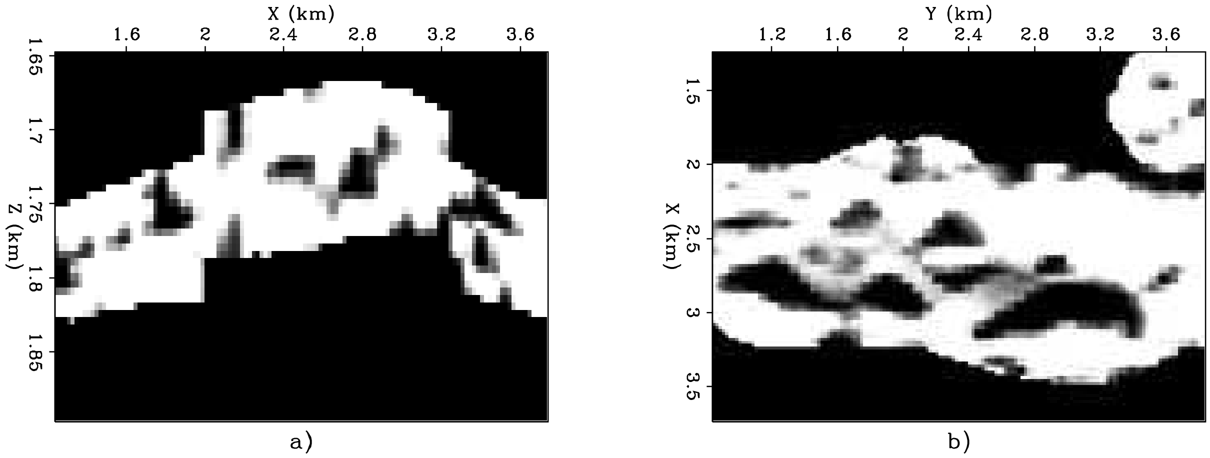

Figure 9: Porosity figures: a) vertical slice at 2270 m, b) Horizontal slice at 1725 m (white high porosity) biondo3-POR [ER]

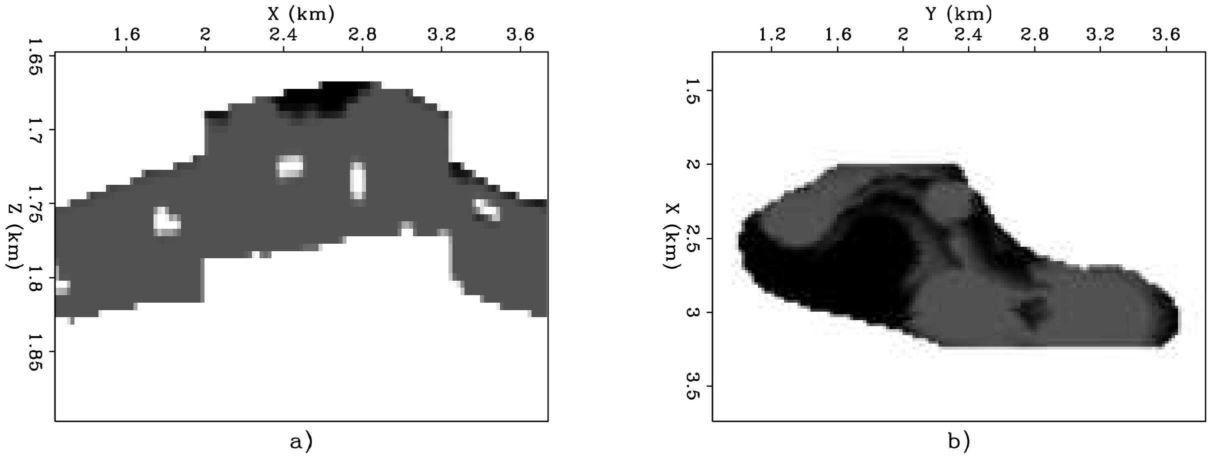

Figure 10: Gas saturation figures: a) vertical slice at 2270 m, b) Horizontal slice at 1690 m showing the reduction of the gas cap through pressure maintenance by the water injectors (white high saturation). biondo3-CompSG [ER]

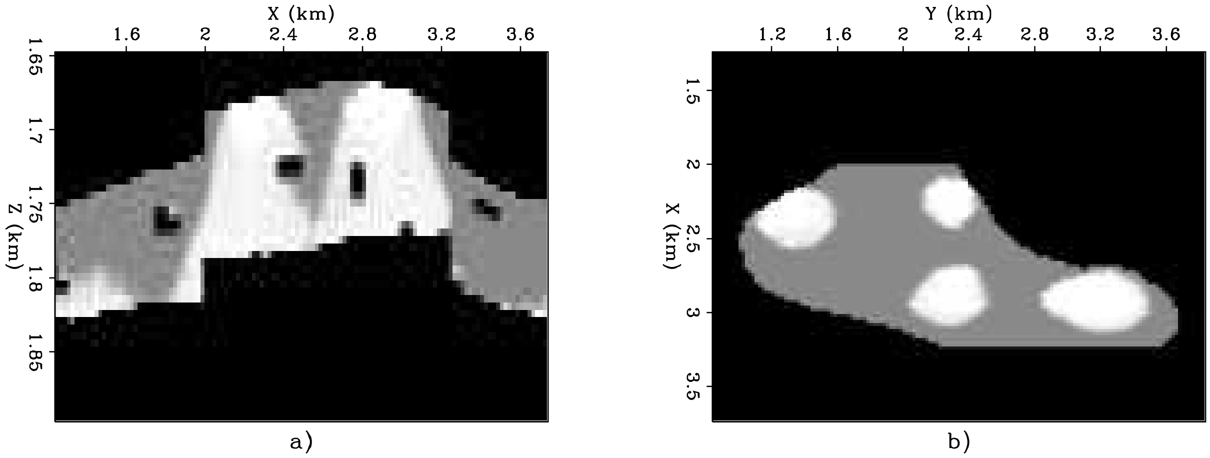

Figure 11: Water saturation figures: a) vertical slice at 2270 m, b) Horizontal slice at 1690 m showing water injection under the effect of gravity and the impact of the nonsealing and sealing faults (white high saturation) biondo3-CompSW [ER]

of importance are lithology, porosity, permeability, pore fluid types and saturations, temperature, reservoir effective stress, and pore fluid pressure. The related bulk properties that most impact seismic wave propagation are bulk density, and P- and S-wave velocities.

Bulk density is the easiest to understand and quantify. Density is the simple volumetric average of all mineral (solid) and pore fluid (solid, liquid, and gas) phases in the rocks. Density changes during reservoir production are primarily the result of replacing the initial set of fluids with another set.

Seismic velocity is always related to the ratio of elastic stiffness of the fluid-bearing rocks to the bulk density of the rocks. The elastic stiffness depends on the mineralogy, the stiffness of the pore space, and the stiffness (incompressibility) K_f of the mixture of pore fluids in the rock. This is most effectively quantified with the well-known Gassmann's equation, which relates the bulk modulus of the saturated rock K_{sat} to the dry rock bulk modulus K_{dry}, the mineral modulus K_0, the fluid incompressibility, and the porosity ϕ:

$$\frac{K_{sat}}{K_0 - K_{sat}} = \frac{K_{dry}}{K_0 - K_{dry}} + \frac{K_f}{\phi(K_0 - K_f)} \tag{4}$$

Important issues when doing fluid substitution:

- frequency: Gassmann's relation is most appropriate for very low frequencies as used in surface seismic. At higher frequencies as used in laboratory ultrasonic and sonic log measurements, fluid effects can give rise to velocity dispersion. This has to be taken into account when using velocity-porosity regressions obtained from such high frequency data. The amount of velocity dispersion depends on the nature of the pore space compressibility. It is enhanced in the presence of soft crack-like pore space, and decreases at high effective pressures when most of the crack-like porosity in closed.

- saturations and heterogeneity: the effective elastic stiffness of the rock depends not only on the saturation (among other things), but also on how the saturation is distributed within the pore space. A saturation distribution that is homogeneous and uniform at the pore scale within each grid block will give a different velocity than a heterogeneous saturation. The two situations require different mixing rules to estimate the effective seismic velocity. For the present exercise, the saturation was taken to be homogeneous within each grid block, and an effective fluid incompressibility (calculated as the Reuss or harmonic average of the individual fluid incompressibilities) was used in Gassmann's equation.

The fluid densities and incompressibilities used in the modeling were obtained from PetroTools Version 2.3, the seismic rock properties software by PetroSoft.

Velocity-porosity regression

Laboratory and sonic log measurements show that velocities usually decrease with porosity, though the velocity-porosity relations are not always unique. P and S velocities are also often well correlated. Velocity-porosity and $V_P - V_S$ regressions have been presented in the literature for different lithologies by various authors. We used similar regressions to define a reference V_P, V_S, and density. For the sand facies we choose a $V_P - \phi$ regression of the form $V_p(km/s) = 3.05 - 1.4\phi$ with a coefficient of variation around the regression of about 2.4%. The $V_P - V_S$ regression was $V_S(km/s) = 0.775V_P - 0.67$, with about 2% coefficient of variation. These are representative of typical water saturated sands from North Sea fields. The regressions (along with the spreads around the regressions) were used to generate the reference V_P and V_S data. We did not include the effect of pressure variations on the $V_P - \phi$ and $V_P - V_S$ regressions, though the effect of pressure on the fluid properties was taken into account. The reference velocities were transformed, applying Gassmann's equations, to the reservoir conditions using the pressure, saturations, and Gas-Oil ratio obtained from the flow simulator. This was done at each time step of interest in the reservoir production history. The fluid incompressibilities and densities as a function of pressure and Gas-Oil ratio were calculated from published laboratory relations incorporated in PetroTools Version 2.3. For the shale facies, which was assigned a zero porosity and negligible permeability, we assigned fixed V_P, V_S, and density of 2.5 km/s, 1.3 km/s, and 2.27 gm/cc respectively. Anisotropy of seismic velocities was neglected in this initial model.

Upscaling-Downscaling

One of the tasks involved mapping the flow simulator output onto a regular Cartesian grid appropriate for seismic modeling. The flow simulator results are defined on a stratigraphic coordinate system with variable block sizes, usually larger than the seismic blocks. The porosity which is defined at the geologic model scale is also on an irregular stratigraphic coordinate system but with blocks smaller than the seismic scale. For upscaling the porosity to the seismic scale, a simple volumetric block averaging was used. The flow simulator outputs were downscaled to the seismic blocks by linear interpolation, first along the depth direction, and then in each horizontal layer. This exercise highlighted the need for better methods of upscaling not only the rock and reservoir properties, but also the rock physics relations between these properties and the seismic observables.

SEISMIC MODELING AND IMAGING

Choice of modeling technique

Seismic modeling of the reservoir required a technique that could handle an Earth model that is both elastic and heterogeneous. This restricted the choice of method available to us.

Zoeppritz or reflectivity methods were not useful as they can only model homogeneous plane layers and cannot capture the effect of heterogeneities. Also finite difference or spectral methods were not useful as they are too computationally intensive for modeling a full multi-offset 3-D survey. This suggested a ray-based scattering approach, such as the first order Born approximation as described by Wu and Aki (1985). More detailed description of the modeling method and direct comparison with Zoeppritz method can be found in (Rickett et al., 1996).

Born elastic modeling

Each point within the reservoir volume is considered as an independent point diffractor of much smaller size than the wavelength of the incident wave. Formulae for Rayleigh scattering are then used to describe the scattering characteristics of each single diffractor, and a modeled trace can then be constructed as the linear sum of contributions from all the elements within the reservoir.

The important assumptions that have to be made for this technique to be applicable are:

1. The Earth model consists of two parts: firstly, a smoothly varying background medium through which ray-paths can be traced; and secondly, within this there

are high-frequency perturbations or point diffractors which act to scatter the wavefield.

2. The amplitude of the perturbations are small relative to the background medium. This allows each scatterer to be treated independently (first order Born approximation). It also means that the scattered wavefield can be modeled as being linearly related to the amplitude of the perturbations.

3. The physical size of scatterers is small with respect to the wavelength of the incident wave, or $ka \ll 1$, where k is the wavenumber of the incident wave and a is the length scale of the heterogeneity.

Following this approach, the field recorded at the surface can be approximated by the following integral taken over the whole reservoir:

$$U(t) = \int A_s \, A_r \, R \, D \, \frac{d}{dt} \, \psi(t - \tau_r - \tau_s) \, dV \tag{5}$$

where A_s and A_r are the geometric spreading factors from the source to the diffractor and from the diffractor to the receiver, D is a correction for the directionality of the receiver, τ_r and τ_s are ray-traced travel-times from the source to the diffractor and from the diffractor to the receiver, $\psi(t)$ is the source signature, and R is amplitude from Rayleigh scattering which can be calculated from the average perturbations $\bar{\delta\rho}$, $\bar{\delta\lambda}$ and $\bar{\delta\mu}$ from the background Lamé parameters ρ_0, λ_0 and μ_0 and the total scattering angle, θ

$$R = \frac{\bar{\delta\rho}}{\rho_0} \cos\theta - \frac{\bar{\delta\lambda}}{\lambda_0 + 2\mu_0} - \frac{2\bar{\delta\mu}}{\lambda_0 + 2\mu_0} \cos^2\theta$$

Calculation of R, τ_r and τ_s can be facilitated by precalculating and tabulating travel-times, geometric spreading factors and propagation angles so that they can be quickly referenced from the inner-loop of the modeling program and do not have to be calculated each time on the fly.

Seismic synthetic data sets modeling and processing

Two seismic surveys were computed over a 2×3 km central block of the modeled reservoir. The first survey was recorded at the beginning of production (t_0), and the second one was recorded after 3 years of production, and two years and a half of water injection (t_1). The data sets covered an area 6×6 km, with 30 m spacing between common-midpoints (CMP's) in both directions. Each data set contains two different offsets (source-receiver distance): zero offset and 3 km offset. Multi-offset surveys allow the analysis of amplitude variation with offset (AVO), which can be useful for identifying variations in the fluid type. The background velocity function was linearly increasing with depth, starting from a velocity of 2 km/s and a constant gradient of .28 s^{-1}.

The wavelet used in the modeling had a maximum frequency of about 45 Hz, giving a wavelength of about 50 m in the target. This is reasonable, but a lower limit on the resolution expected for a target of this depth. Further modeling will be done with higher frequencies.

The modeled data was imaged using a Kirchhoff 3-D prestack migration program. The kinematics and amplitudes used by the migration were obtained by numerically tracing rays through the given background velocity function. The migration code had the appropriate anti-aliasing corrections and amplitude tapering to preserve the correct amplitudes. The two different offsets (0 and 3 km) present in the data sets were migrated and analyzed separately.

SEISMIC MONITORING RESULTS

We present the seismic imaging results from the zero-offset data side-by-side with the corresponding seismic effective properties used as input to the seismic modeling and imaging procedure. To enable direct comparisons, we show sections through the acoustic impedance cube and through its estimates derived from the seismic migration results. These impedance estimates were simply obtained by integration along the depth axis of the migration results.

Figure 12 shows vertical sections through the acoustic impedance cube taken at cross-line 2.27 km where two water-injecting wells were located. The sections on the top show the "impedance" values at t_0, while the sections in the middle show the values at t_1. The bottom sections show the values at t_0 subtracted from the values at t_1. The effects of the water injection, which causes the gas cap to be unevenly depleted are apparent from the seismic images.

The spatially heterogeneous nature of the gas-cap depletion process is also evident from the horizontal slices shown in Figure 13, taken at a depth of 1.69 km. This images correlate very well with the images showing the gas saturation (Figure 10) and water saturation (Figure 11) in the reservoir. The relative low-frequency, and consequently low resolution, of our surveys prevents the migration to image the spatial heterogeneities at the same level of details present in the seismic impedance model. This observation confirms that reservoir monitoring does indeed require the use of advanced seismic acquisition and processing technologies aimed at maximizing the resolution of the final seismic images.

Figure 14 shows the horizontal slices taken deeper in the reservoir (1.725 km). The effects of the formation of a small gas cap on the side of the sealing fault are apparent in both difference sections. The formation of this gas cap can be also seen in the vertical slice through the gas saturation field (Figure 10a) and the vertical slice through the seismic properties (Figure 12a)). Another apparent feature of his horizontal slices are the low-permeability shale bodies, also visible in the porosity section (Figure 9b). These areas of the reservoir show very low values in the difference section, since low-permeability prevents large changes in fluid properties and are potential barriers to fluid-flow .

Figure 15) shows the potential additional information that can be obtained from imaging non-zero offset data. It show the same sections shown in Figure 12b, together with the equivalent section resulting from the migration of the 3 km offset data. As expected from migration theory, the results computed from non-zero offset data (Figure 15b) have lower resolution than the ones computed from zero-offset data (Figure 15a). However, beside this resolution mismatch, the variations with offset in the seismic response of gas-saturated sand is apparent from the Figure. These differences are mostly visible at t_0 when the gas cap was not depleted, and in the difference section in which the effects of the water injecting wells are enhanced.

The results of the seismic imaging and modeling process suggest that fluid-flow patterns and variations of fluid properties within the reservoir can be detected using 3-D seismic surveys. However, conclusions should be drawn cautiously from these results since they were not affected by all the factors that in a real case would contribute to degrade the results of seismic imaging; such as: noise, acquisition constraints, and uncertain knowledge of the overburden parameters.

FUTURE CONSIDERATIONS

The main goal of this project was to begin a collaborative effort between various disciplines including (1) geological reservoir modeling (2) fluid flow simulation (3) rock physics, and (4) seismic imaging to explore and understand how reservoir monitoring may be used as a tool for efficient reservoir management. Seismic monitoring promises to provide valuable information about reservoir fluid movements and reservoir geological heterogeneities. However, issues of resolution, scales, and uncertainties need to be explored.

Our preliminary results warrant further research in this direction. Future work will address the following issues:

- Using seismic monitoring to constrain geological models and reduce the uncertainty in reservoir performance forecasting. In the context of stochastic reservoir modeling, flow simulation is performed with alternative equally-probable reservoir geologic models. The uncertainty in future reservoir performance is measured by the differences in flow simulation outcomes. The information provided by seismic monitoring data will possibly reduce this uncertainty by constraining the reservoir geological models.

- In this study we performed steps A through D of the reservoir-to-seismic modeling flow loop shown in Fig. **??** on a single geological realization. Future work should address the computationally challenging issue of closing this loop by considering multiple geostatistical realizations. This task will be feasible only if

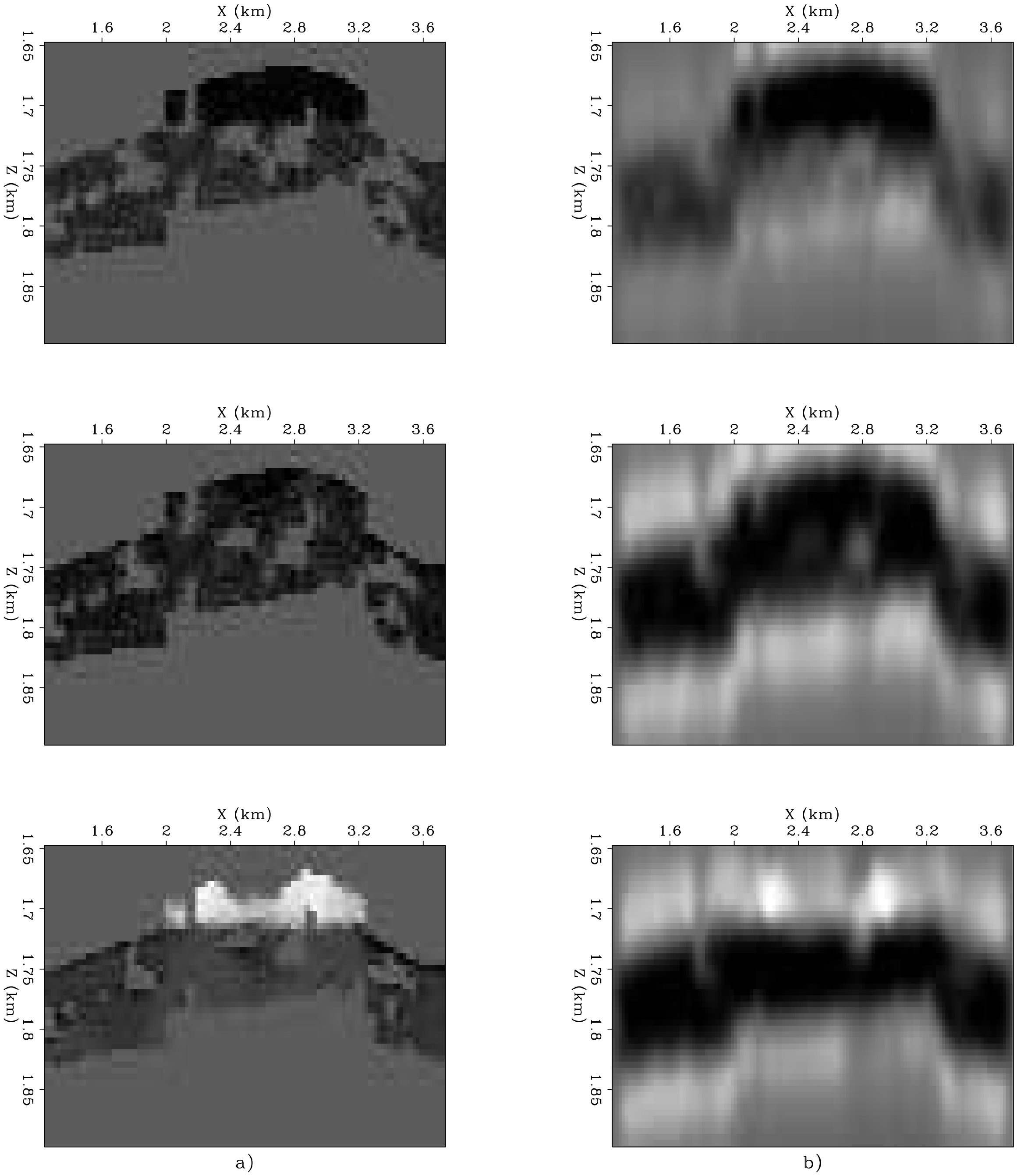

Figure 12: Vertical slices at cross-line 2.27 km. Left panels show acoustic impedance model, right panels show the results of seismic imaging. Top row is at t_0, middle row is at t_1, and bottom row is the difference between the two. biondo3-Compv72 [CR]

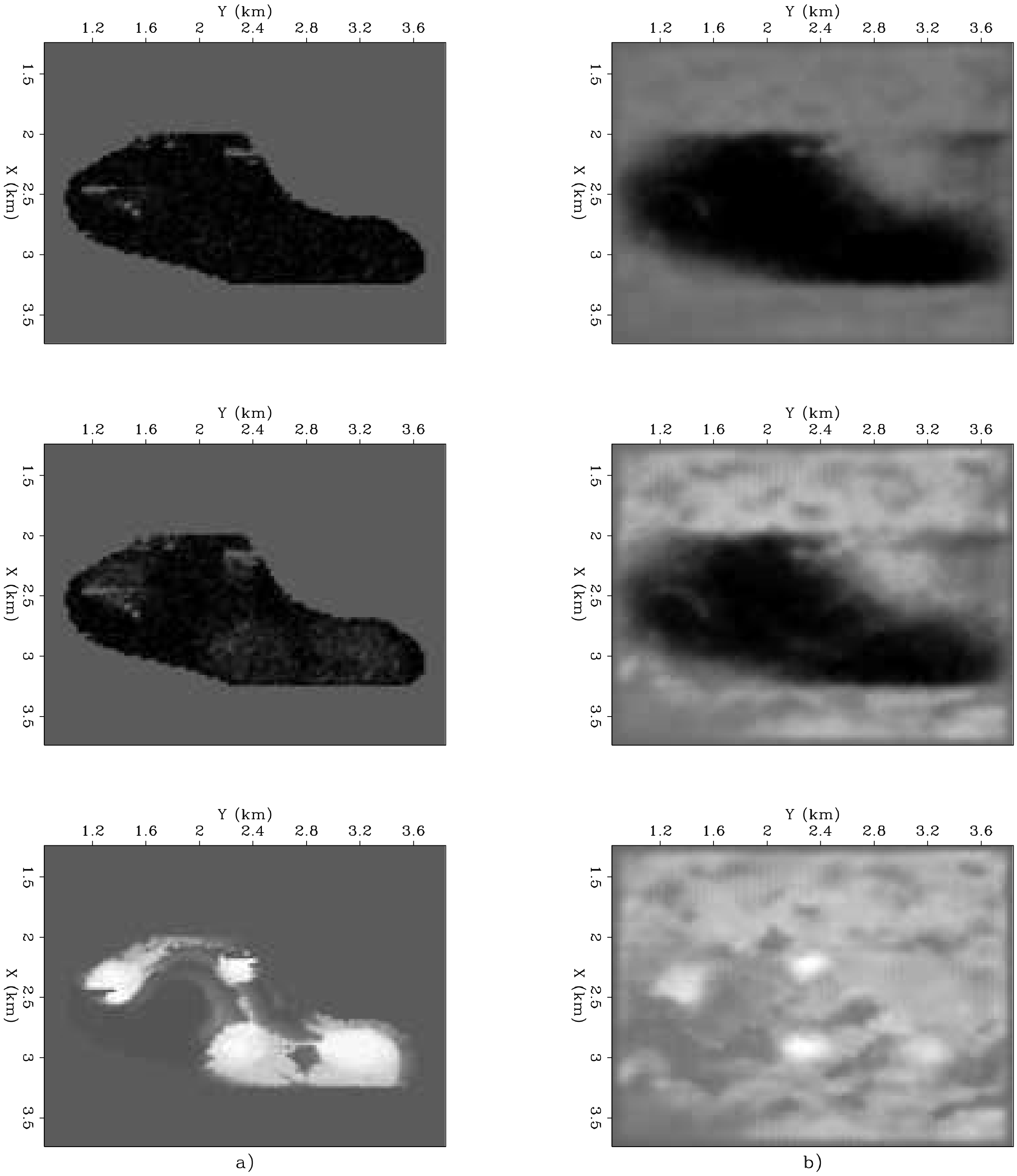

Figure 13: Horizontal slices at 1.690 km depth. Left panels show acoustic impedance model, right panels show the results of seismic imaging. Top row is at t_0, middle row is at t_1, and bottom row is the difference between the two. biondo3-Comph8 [CR]

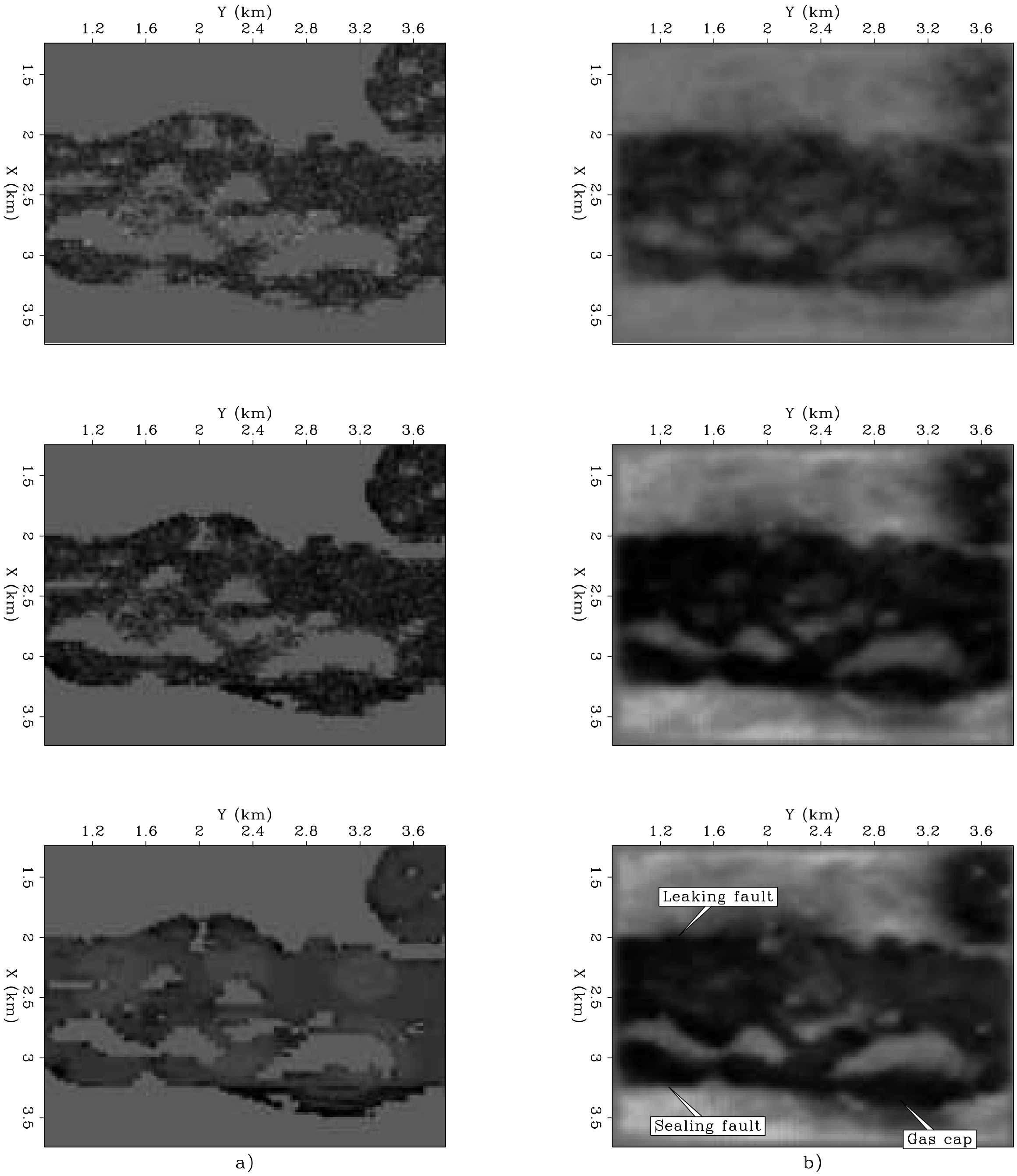

Figure 14: Horizontal slices at 1.725 km depth. Left panels show acoustic impedance model, right panels show the results of seismic imaging. Top row is at t_0, middle row is at t_1, and bottom row is the difference between the two. biondo3-Comph15 [CR]

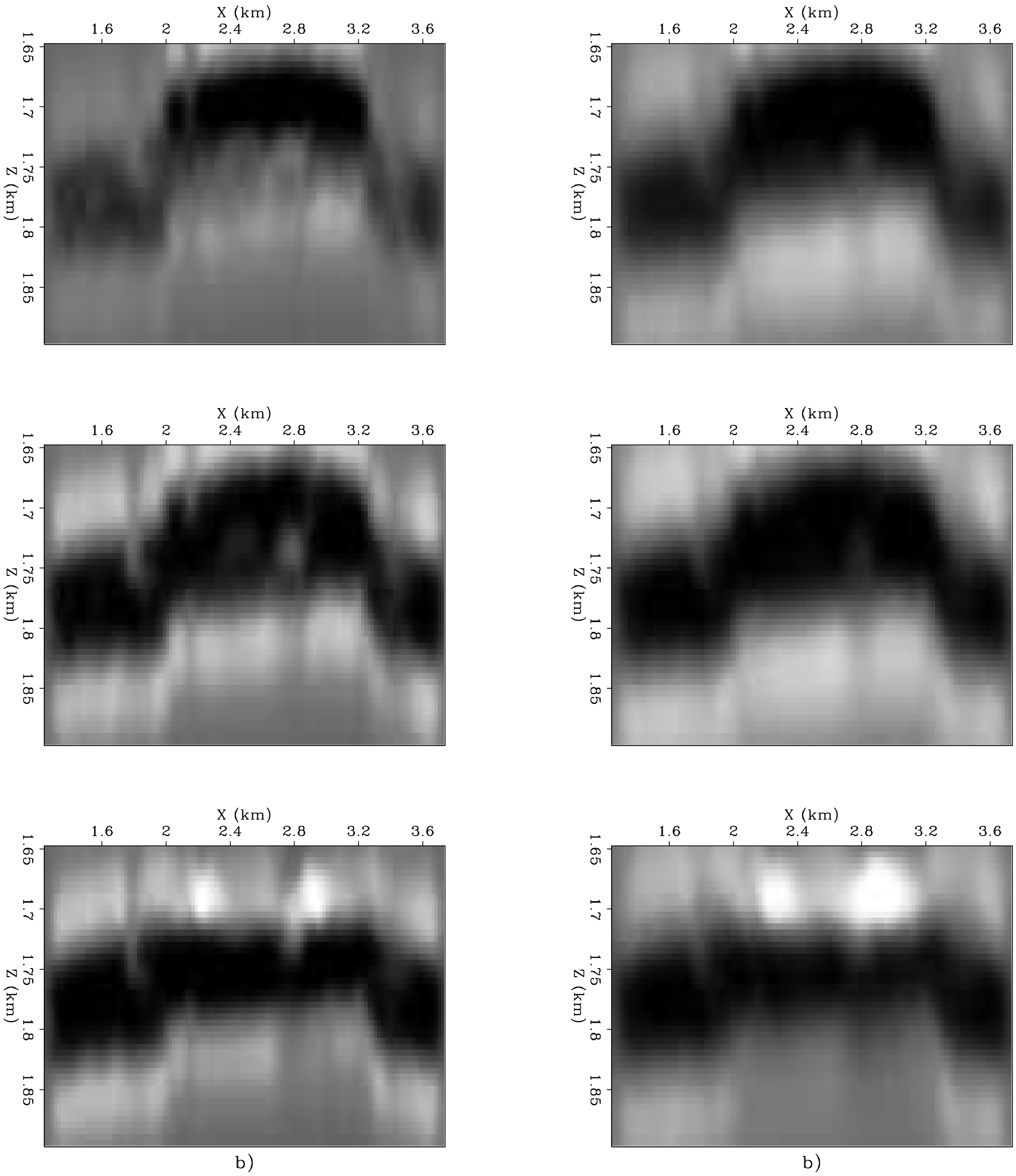

Figure 15: Vertical slices at cross-line 2.27 km. Left panels show the result of imaging the zero-offset surveys, right panels show the result of imaging the 3 km offset surveys. Top row is at t_0, middle row is at t_1, and bottom row is the difference between the two. biondo3-Compv72o3000 [CR]

sufficient resources are available for the computationally intensive seismic imaging and fluid flow simulations, and efficient algorithms are developed to model the process with an acceptable resolution at the relevant scales.

- Estimating uncertainties due to non-unique assignment of acoustic properties from the reference lithofacies, porosity, and saturations. Laboratory experience has demonstrated that seismic properties depend not only on pore fluid saturations, but also on the scales of their spatial distributions. The impact of this at field scales must be explored. This project highlighted the need for better methods of upscaling not only the rock and reservoir properties, but also the rock physics relations between these properties and the seismic observables.
- At the essence of seismic monitoring is the capability of analyzing the differences between seismic images obtained from data sets recorded at different times, with possibly variable acquisition geometry, waveform, bandwidth, and coherent noise. Methods to remove the effects of all these perturbations must be developed to enable seismic monitoring to reduce the uncertainties of reservoir characterization.

We envision that future work in this area will (1) build on the multi-disciplinary collaboration already started, involving students from the different departments (2) consider real reservoir data, and (3) provide fertile grounds for applicable solutions to reservoir management problems.

ACKNOWLEDGEMENTS

We would like to thank Silicon Graphics for loaning a 16-processors Power Challenge that has been the main computational platform for the project.

We also would like to thank GeoQuest for making Eclipse available on the Power Challenge, and Jon Norris for installing and helping us run the code.

REFERENCES

Lumley, D., Nur, A., Strandenes, S., Dvorkin, J., and Packwood, J., 1994, Seismic monitoring of oil production: A feasibility study: SEP–**80**, 209–262.

Rickett, J., Biondi, B., and Lumley, D., 1996, Modeling heterogeneous reservoirs using the first order Born approximation: SEP–**92**, 75–82.

Wu, R., and Aki, K., 1985, Scattering characteristics of elastic waves by an elastic heterogeneity: Geophysics, **50**, no. 4, 582–595.